# Analysis and optimization of a wire actuated, single effect n-R robotic structure

Alain Favetto†,‡,*, Silvia Appendino†,
Alessandro Battezzato†, Fai Chen Chen†,§,
Mehdi Mousavi†,§, Francesco Pescarmona†
and Giuseppe Carlo Calafiore‡

†*Istituto Italiano di Tecnologia IIT@Polito, Center for Space Human Robotics, Corso Trento 21,
10129 Turin, Italy*
‡*Dipartimento di Automatica e Informatica, Politecnico di Torino, Corso Duca Degli Abruzzi 24,
10129 Turin, Italy*
§*Dipartimento di Meccanica, Politecnico di Torino, Corso Duca Degli Abruzzi 24, 10129 Turin,
Italy*

## SUMMARY
This paper investigates the kinematics and the optimization of a generic robotic structure composed by N serial rotary joints and actuated with a mono-directional tendon system. In the first part of the paper, the specific case that brought us to develop this study is introduced; the main motivations and the scenario with its specific constraints and design choices have been described.

Since a complete and detailed analysis of an n-R serial structure with this kind of characteristics could not be found in the literature, the study of the kinematics and the parameter optimization of such a structure is treated as generally as possible, in order to make the procedure and the results applicable for any similar structure. Finally, in the last part, through the introduction of specific constraints and the definition of the parameters, the general analysis has been applied to the specific case of study: the preliminary study of a finger exoskeleton for an astronaut suit.

KEYWORDS: Exoskeletons; Biomimetic robots; Grasping; Design; Space robotics.

## 1. Introduction
Robotic structures can differ from each other for their initial requirements and constraints, for their general architecture, and finally for the elements that compose it, mainly actuation and transmission.

This paper focuses on a wire actuated single effect robotic structure. This kind of actuation system was chosen in order to minimize the dimensions and weight of the final device, since bulk is a fundamental constraint for our specific project.

Cable (or wire, or tendon) actuation is widely used in robotics, and in particular for parallel manipulators or robotic hands. Several examples of parallel manipulators can be found in the literature: the WiRo[1,2], WARP,[3] NIST Robocrane,[4] Falcon-7.[5] Extensive theoretical work has been performed by Merlet.[6–8] Regarding robotic hands, the Shadow Hand[9] and the DLR-Hand II[10] are two very important examples of the state of the art.

The main advantage of using wire actuation is the opportunity to lighten the most critical points, by placing the actuators elsewhere. This is evident in the Shadow Hand, where all the actuators, i.e., pneumatic muscles, are placed in the forearm thus realizing a human sized robotic hand. On the other hand, the main inconvenience of wire actuation is that cables can only work by traction: therefore, special solutions are required to obtain the complete control of each degree of freedom (DoF).

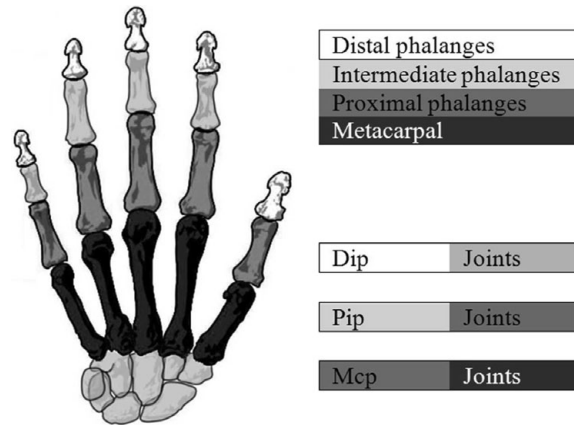* Corresponding author. E-mail: alain.favetto@polito.it

Fig. 1. Articulations and phalanges of the human hand.

In order to overcome the problem of traction and to reduce the complexity of the device, single effect actuation is considered. Therefore, each DoF of the robotic structure is actuated actively only in one direction, while the recall movement is effected through passive elements, e.g., elastic components.

### 1.1. Specific project and motivation

This research activity arose from a larger project which aims to produce a hand exoskeleton to help astronauts overcome the stiffness of the suit glove while conducting extra vehicular activities (EVA).[11]

Hand exoskeletons present in the literature are usually developed for rehabilitation, as medical prostheses or as human–machine interfaces and are often characterized by a reduced number of DoFs, by large dimensions and weight. Small dimensions and a low weight are however fundamental aspects of our project, which thus requires a different conceptual and technological approach.

As mentioned before, wire actuation allows dimensions and weight to be reduced by keeping the actual device unhampered. Moreover, the placement of the actuation system in a noncritical position means that it can be neglected completely during the first steps of the design, and its actual definition postponed. Furthermore, the intrinsic stiffness of the EVA glove, due to its multiple layers and its internal pressurization, allows the realization of a single effect strategy, since the glove itself can act as the passive elastic element for the return stroke.[12–17] This choice simplifies the structure and the actuating system greatly and contributes, in part, to achieving the goal of lightness and reduced dimensions.

In this paper, the conceptual design of the robotic structure has been generalized as much as possible and separated from the specific design of the hand exoskeleton. This generalization permits to apply the analysis to different designs and structures, provided that they adhere to the conceptual choices explained in the following.

## 2. Concepts Behind the First Design

In order to simplify the approach toward a hand exoskeleton we decided to start from a single finger exoskeleton: in the future, this study will be generalized for all the other fingers of the device.

All the requirements for the whole hand exoskeleton are however considered in the single finger device: it has to support the finger movements, to ensure the correct kinematics and it must not interfere with the palm or with the other fingers of the hand. It is important to underline that this first design aims to minimize dimensions and weight.

The single effect finger exoskeleton is actuated only in flexion and utilizes passive components, e.g., elastic elements (or the EVA glove itself) for the extension.

This section describes some constraints and design choices which are specific to our project but may contain valid suggestions for other researchers working on similar applications. Moreover, an extension to the more general case is attempted.

### 2.1. Human finger

The human hand is constituted by five digits: four fingers and the thumb. As shown in Fig. 1 the human finger is composed of three articulations, distal-interphalangeal (DIP), proximal-interphalangeal
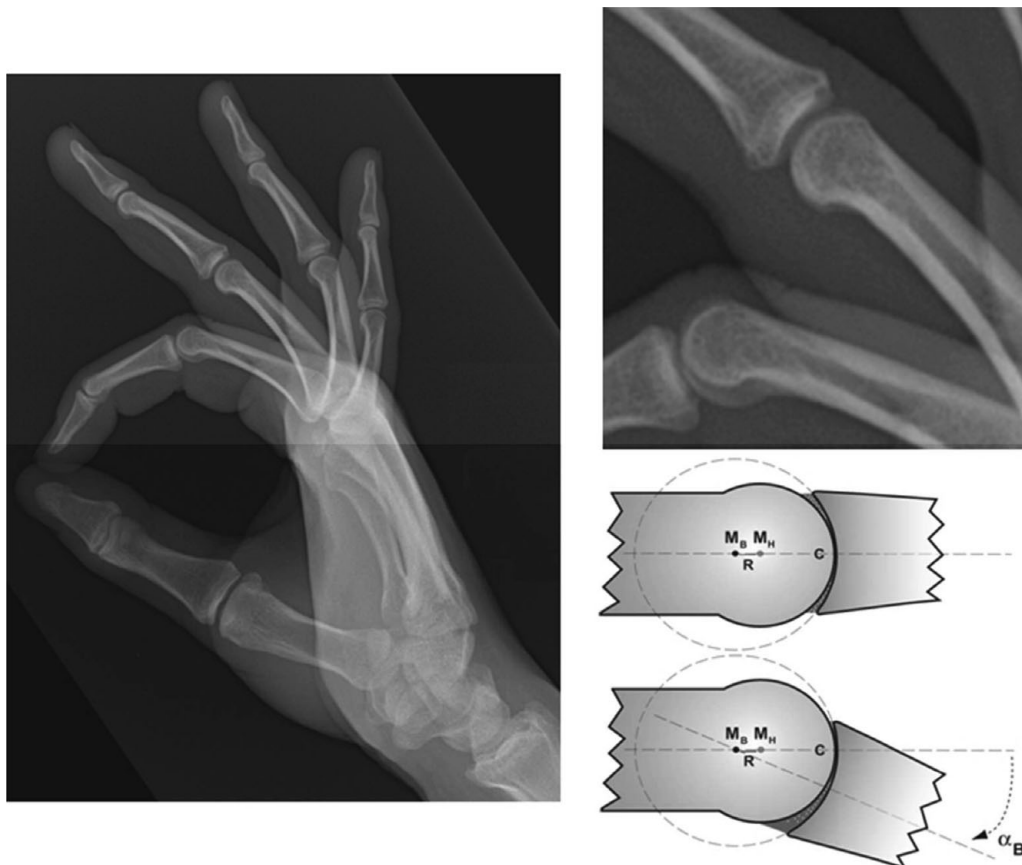
Fig. 2. Human knuckles behavior.

(PIP), and metacarpophalangeal (MCP) and of four phalanges, distal, middle, proximal, and metacarpal phalanx. Each finger can be modeled with a kinematic chain composed off our links and four DoFs. Three of them are related to the flexion–extension movement and one is related to the adduction–abduction movement. The thumb shows a different structure, not specifically addressed here for the sake of brevity. At this stage, the adduction–abduction movement is neglected and kept passive, thus the realized model is composed of only the three DoFs which have parallel axes. The centers of rotation of the joints of the mechanism and the ones of to the corresponding human joints must be coaxial, thus the MCP articulation presents another problem: the crotch. The webbings between fingers impose strong restrictions on the location and shape of the elements of the device, and require the designer to look for nontrivial solutions. The main critical point in the development of a hand exoskeleton is related to the extremely wide hand dexterity, which may not be excessively restricted by the device.

All mentioned concepts can be generalized and applied to different solutions that maintain the general idea of a single effect robotic structure. Moreover, the modularity of the approach presented in this paper means that the concept can be generalized to structures having a generic number of links *n*.

### 2.2. Joints
The human knuckles are not pure rotational joints. They have a behavior which is more similar to a sliding convex–concave couple of profiles with different and varying radii,[18] as shown in Fig. 2. The faithful reproduction of this type of joint is an unnecessary complication in the design and would be excessively demanding in terms of size and weight. A pure rotational joint is an acceptable compromise that guarantees a kinematical behavior which is very similar to the real one, since the human finger has enough flexibility to compensate for such small differences without problems or risks. Three solutions have been analyzed to design pure rotational joints: traditional joints, virtual

Fig. 3. Wire actuation with (left) and without (right) access to the joint.

joints, and no joints. Traditional joints, i.e., a classic coupling of two or more rigid elements, such as a hinge, have the advantage of ensuring the right kinematics, and of allowing the distribution of a large part of the resultant forces directly on the structure. This solution is demanding in terms of dimension and weight. Real (traditional) joints are widely used both on hand exoskeleton and robotic hands; Shadow Hand,[9] the DLR-Hand II,[10] and HANDEXOS[19] are only few examples. The jointless solution, using human joints only, is the best one in terms of dimension and weight, but has some disadvantages. First of all the resultant forces act on the finger articulation, and only the human finger guarantees the correctness of kinematics. This solution results unsuitable for robotic hands; it is adopted mainly in low power exoskeleton design, DiCicco's orthotic exoskeleton[20] and Li Jiang's haptic exoskeleton[21] are a couple of examples. Finally, virtual joints are elements that ensure kinematics without being true joints, such as elastic components, e.g., flexures. They are a compromise between the traditional joints and the joint less solutions. In literature there are several examples, in particular the work of Berselli *et al.*[22] shows an overview of some compliant and elastic joints for robotic structures.

The analysis presented in this paper can be applied to any joint solution, provided that there is an element, which ensures extension movements, e.g., an elastic element, in order to apply the concept of "single effect."

### 2.3. Transmission
Although our specific aim is to design a finger exoskeleton structure, it is paramount to stress the fact that this study can be applied to any single effect n-R planar arm, no matter what its proportions or scopes are.

The transmission proposed in this paper is achieved by mono-directional tendons (wires), which pull each phalanx (or link) only in its flexion movements. The extension movement is guaranteed by passive elements coaxial with the joints, such as a torsion spring or any element that can be modeled like an elastic component, e.g., the intrinsic stiffness of the EVA glove. Tendon transmission permits to place the actuation system in a noncritical position, thus the actuation itself is not treated in this study.

The solution proposed in this paper considers that the actuation and transmission system cannot be directly linked to the joints. The wires pass through the links and are fixed to their "final" link without guaranteeing a fixed arm with respect to the joints. This assumption permits to generalize the concept for solutions with virtual joints and "no joints," where it is not possible to impose the passage of the cables in a fixed point of the joint. This choice has two main consequences: the minimum distances between the cables and the joints will not remain fixed during movements, and the passage of the cables through the center of rotation of the joints cannot be imposed. Figure 3 shows the differences between the classical wire actuation with access to the joint (left) and the solution proposed in this paper with no access to the joint (right).

These assumptions imply that the movements of the joints cannot be decoupled from one another, thus transmission of the joint *i* also acts on the previous *i*–1 joints.

### 2.4. Global overview
The above discussion provides a series of motivations for each choice and a functional idea of each element of the physical device. This means that a family of devices could be unified under the same previously treated "guidelines," independently from the technological solutions. The choices to place real springs or not, to allow the passage of the cables with micromachined holes rather than micropulleys are examples of different technological solutions for the same concept with different advantages and disadvantages.
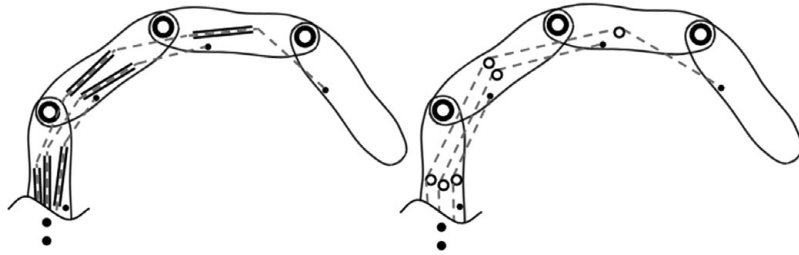
Fig. 4. Concept structure with micro-machined holes (left) and with micro-pulleys (right).
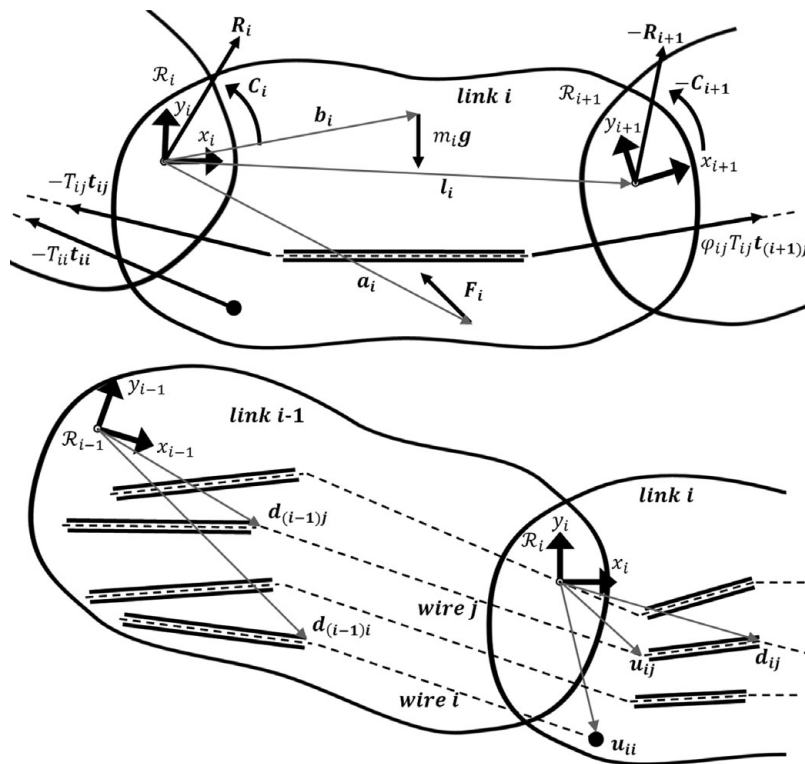


Fig. 5. Link schemes.

Figure 4 represents the conceptual scheme under study. Each link of the robotic arm is represented by a rounded block; in the actual design these blocks can have any shape and size. Two adjoining blocks are linked together with a pure rotational joint that can be real, virtual or fictitious (in the case of "no joint" solution). An elastic component (not represented in the pictures) is placed inside each joint in order to guarantee the extension movement.

A certain number of tendons pass through each block. They are used to transmit motion, depending on the position of the block in the kinematic chain. The passage of the wires through the links can be achieved in different ways. Figure 4 shows two examples, i.e., micromachined holes (left) and pulleys (right). Other solutions are also possible.

It is important to underline that this model is planar and with all the axes parallel to each other. Axes with a different orientation (e.g., the abduction–adduction DoF in the specific case of human finger) cannot be placed inside the kinematic chain, but rather can be treated separately and added upstream.

## 3. Statics

Figure 5 represents the scheme of the generic $i$th link of the robotic structure. Each link is associated with a coordinate reference system $\mathcal{R}_i$ which uniquely defines its position and orientation. In this

study the apex $i$ on the generic vector $^i\boldsymbol{x}$ states that the vector is expressed in the $i$th reference frame $\mathcal{R}_i$. The $i$th reference system is placed on the $i$th rotational joint, which connects the $i$th link to the previous one. $\mathcal{R}_i$ can be obtained from $\mathcal{R}_{i-1}$ through a translation represented by the position vector $^i\boldsymbol{l}_{i-1}$ and a subsequent rotation around it of an angle $\theta_i$. Each link is driven by a corresponding wire. The architecture consists of a serial chain of $N$ links, each of them hosting the holes for the wires that drive the following elements. Hence, as shown in Fig. 5, $N+1-i$ wires enter the $i$th link from the previous one, while $N$-$i$ of them go to the following link. The wire $i$ acts specifically on the link $i$ and ends there. The generic wire $j$ $(j > i)$ enters the link $i$ coming from the previous one and continues to the following one. If the wire does not pass exactly through the origin of $\mathcal{R}_i$, it has a non-null torque effect on the $i$th link, which must be controlled and optimized. The position vector that identifies the entrance of the hole for the generic $j$th wire in the $i$th link is called $^i\boldsymbol{u}_{ij}$ ($u$ for upstream). The position vector of the end of the same hole is referred to as $^i\boldsymbol{d}_{ij}$ ($d$ for downstream). It is important to underline that by imposing $^i\boldsymbol{d}_{ij} = {}^i\boldsymbol{u}_{ij}$, one obtains the specific case in which the passage of the wires is performed trough micropulleys rather than micromachined holes. $^i\boldsymbol{t}_{ij}$ is the unit vector that identifies the direction of the generic $j$th wire on the $i$th link, and it is defined as follows:

$$
^i\boldsymbol{t}_{ij} = \frac{^i\boldsymbol{u}_{ij} + {}^i\boldsymbol{A}_{i-1}\left(^{i-1}\boldsymbol{l}_{i-1} - {}^{i-1}\boldsymbol{d}_{(i-1)j}\right)}{^i\boldsymbol{u}_{ij} + {}^i\boldsymbol{A}_{i-1}\left(^{i-1}\boldsymbol{l}_{i-1} - {}^{i-1}\boldsymbol{d}_{(i-1)j}\right)},
\tag{1}
$$

where $^i\boldsymbol{A}_{i-1}$ is the linear operator which maps vectors and points from the reference $\mathcal{R}_{i-1}$ to the reference $\mathcal{R}_i$.

$$
^i\boldsymbol{A}_{i-1} = \begin{bmatrix} \cos(\theta_i) & \sin(\theta_i) \\ -\sin(\theta_i) & \cos(\theta_i) \end{bmatrix}
\tag{2}
$$

and $\theta_i$ is the counterclockwise angle between $\mathcal{R}_{i-1}$ and $\mathcal{R}_i$.

The generic $i$th link is subject to the following forces and torques, depicted in Fig. 5:

- $^i\boldsymbol{R}_i$ and $^i\boldsymbol{C}_i$, exerted by the previous link at the $i$th joint
- $-^i\boldsymbol{R}_{i+1}$ and $-^i\boldsymbol{C}_{i+1}$, exerted by the following link at the $(i+1)$th joint
- $^i\boldsymbol{F}_i$, external force applied on the $i$th link (e.g., exerted by the user), whose point of application is identified by vector $^i\boldsymbol{a}_i$
- $m_i\boldsymbol{g}$, link weight applied in its center of mass, identified by vector $^i\boldsymbol{b}_i$. Vector $g$ is gravity, typically expressed in the fixed, or 0th, reference system: $^0\boldsymbol{g}$
- $-T_{ij}{}^i\boldsymbol{t}_{ij}$, tension exerted by the $j$th wire, whose point of application is given by the vector $^i\boldsymbol{u}_{ij}$. Given that the force is a traction one, its direction is opposite to the unit vector $^i\boldsymbol{t}_{ij}$, while its magnitude is $T_{ij}$. The index $j$ varies from $i$ to $N$
- $\varphi_{ij}T_{ij}{}^i\boldsymbol{t}_{(i+1)j}$, tension exerted by the $j$th wire, whose point of application is given by the vector $^i\boldsymbol{d}_{ij}$. Its direction coincides with the unit vector $^i\boldsymbol{t}_{(i+1)j}$, while its magnitude is $\varphi_{ij}T_{ij}$. The coefficient $\varphi_{ij}$ is a factor that considers the reduction of force along the $j$th wire due to the friction associated with the sliding of the wire into the hole. The index $j$ varies from $(i+1)$ to $N$.

A study of the coefficient $\varphi_{ij}$ follows. When the wires pass inside their holes, they are bent by a certain angle. In practice it will not be a sharp corner because the hole's extremity will be rounded, therefore the effect of friction at the bend can be studied according to the theory of belts. Figure 6 depicts this friction effect, which reduces the tension of the wire twice per hole, at the entrance and at the exit.

The total effect of friction in the hole[23] is equal to:

$$
\varphi_{ij} = \frac{\varphi_{ij}T_{ij}{}^i\boldsymbol{t}_{(i+1)j}}{-T_{ij}{}^i\boldsymbol{t}_{ij}} = \mathrm{e}^{-f(|\alpha_{ij}|+|\beta_{ij}|)}.
\tag{3}
$$

The constant $f$ is the Coulomb friction coefficient between wire and hole walls, which can be evaluated experimentally or extracted from literature data, and depends on the materials and on the
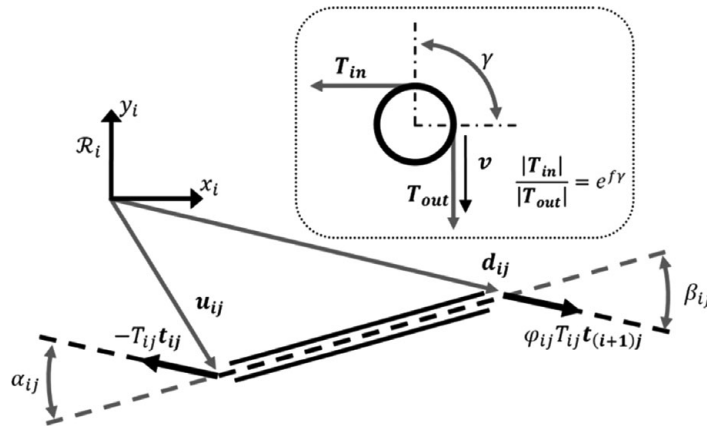
Fig. 6. Friction due to the sliding of the wires inside the holes.

contact geometry. The two bending angles $\alpha_{ij}$ and $\beta_{ij}$ can be calculated as follows:

$$\alpha_{ij} = \arccos\left[\frac{{}^i t_{ij} \cdot \left({}^i d_{ij} - {}^i u_{ij}\right)}{{}^i d_{ij} - {}^i u_{ij}}\right]; \quad \beta_{ij} = \arccos\left[\frac{{}^i t_{(i+1)j} \cdot \left({}^i d_{ij} - {}^i u_{ij}\right)}{{}^i d_{ij} - {}^i u_{ij}}\right]. \tag{4}$$

Thus, the equations of the translational (5) and rotational (6) equilibrium of the generic *i*th link can be written as:

$$
{}^i R_i - {}^i R_{i+1} + m_i {}^i A_0 {}^0 g + {}^i F_i - \sum_{j=i}^{N} T_{ij} {}^i t_{ij} + \sum_{j=i+1}^{N} \varphi_{ij} T_{ij} {}^i A_{i+1} {}^{i+1} t_{(i+1)j} = 0 \tag{5}
$$

$$
{}^i C_i - {}^i C_{i+1} - {}^i l_i \wedge {}^i R_{i+1} + m_i {}^i b_i \wedge {}^i A_0 {}^0 g + {}^i a_i \wedge {}^i F_i
$$

$$
- \sum_{j=i}^{N} {}^i u_{ij} \wedge T_{ij} {}^i t_{ij} + \sum_{j=i+1}^{N} {}^i d_{ij} \wedge \varphi_{ij} T_{ij} {}^i A_{i+1} {}^{i+1} t_{(i+1)j} = 0. \tag{6}
$$

The equations of the *i*th link require the solutions of the following $N-1$ links to be solved.

## 4. Optimization

The optimization process aims to find the best set of parameters in order to minimize internal stresses and to limit the range of tendon tensions. However, the definition of "best" is not univocal. In some cases it could mean limiting the peak of a specific internal variable, in other cases reducing oscillation by keeping a variable as constant as possible. Using the kinematic relationships between parameters (see Eqs. (5) and (6)) the set of values of parameters that optimizes a certain target can be called the "best" configuration of the tunable parameters. A wide and comprehensive study related to the manipulators and grasping device in terms of modeling, constraints and optimization criteria can be found in the work of Ceccarelli[24] and Carbone *et al.*[25−27]

Sections 4.1.1 and 4.1.2 will analyze all the elements involved in the optimization process and present some possible optimization choices. The magnitude of tendon tensions is one of the main quality factors of this specific project. In any case, the generic tension $T_i$ must be limited between two values:

$$T_{\min} < T_i < T_{\max}, \tag{7}$$

where $T_{\min}$ is the minimum acceptable wire tension value. This must be positive, and to increase the controllability margin a value of $T_{\min}$ greater than zero has to be introduced in order to compensate undesired effects or nonidealities. $T_{\max}$ is the maximum acceptable wire tension value. This is a function of the maximum stress that the wires can undergo and by the maximum value of $T$ that the actuators can (directly or indirectly) produce.
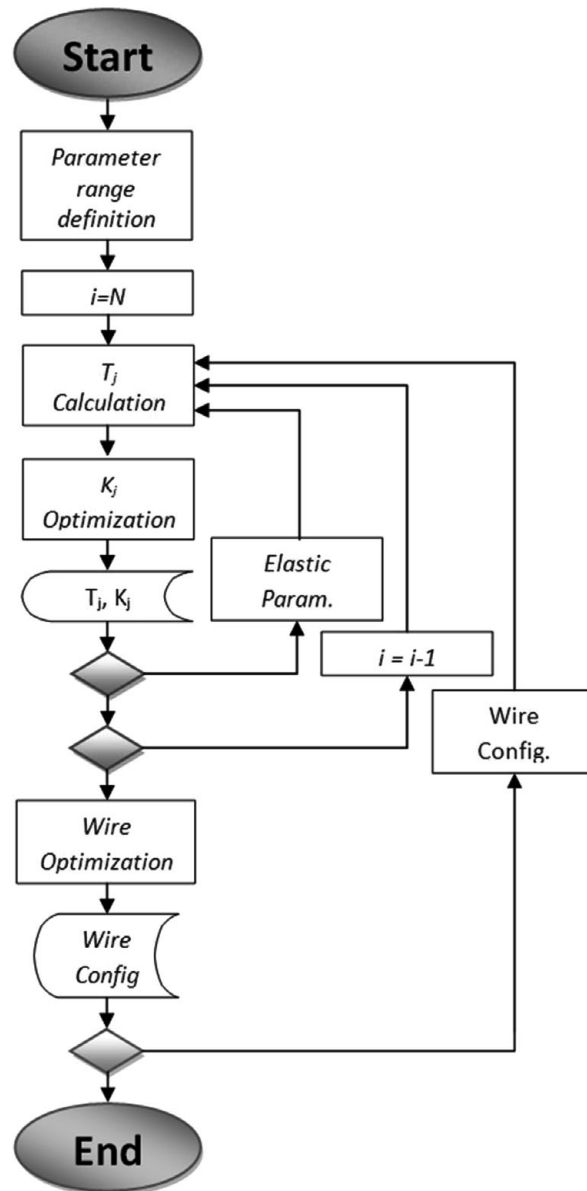
Fig. 7. Flow chart.

There are two typologies of parameters to combine in order to achieve the goals mentioned above:

- *Fixed*: intrinsic and unchangeable parameters specific to each design (e.g., geometrical parameters, position of the joints, DoFs, etc.).
- *Tunable*: parameters that can vary within a determined range of values on the basis of design choices (e.g., the possible positions of the passing points of the wires inside the structure): these can be adjusted for optimization.

It is necessary to underline that different projects, though based on the same concept, can have different sets of fixed and tunable parameters according to the characteristics of the device itself. The distance between two joints is an example of a fixed parameter in an exoskeleton design because the device has to be worn, while it could be tunable for another application.

### 4.1. Algorithm
An algorithm calculates the best possible configuration of the tunable parameters. Figure 7 presents a flow chart describing the main steps of the optimization procedure.

The main tunable parameters for robotic structures according to the previously presented concept are:

- the position of the wire holes inside each phalange of the device
- the parameters of the elastic components (depending on the chosen elastic components)
- the minimum tendon tension range $T_{min}$
- the range of the external force $\boldsymbol{F}$ (if in the specific design it is considered as a tunable parameter).

For each value of $\boldsymbol{F}$ and $T_{min}$ and for each specific wire hole position, an analysis of every possible wire configuration (inside the defined range) is carried out. At the end of this analysis the following values are calculated:

- the elastic parameters that best satisfy the design requirements
- the mean and peak values of the $N$ tendon tensions.

During each iteration (corresponding to a specific wire configuration), the $N$ tendon tensions are calculated and the stiffness values of the elastic components is optimized to find the best configuration.

Due to the superposition effect, the generic $i$th link also applies an effect on the previous $i$-1. The algorithm begins by calculating and optimizing the parameters of the last link (the $N$th), and then proceeds backwards along the kinematic chain.

The first step of the iteration is to calculate the tension $T_i$ of the tendon acting on the link $i$. At this point all parameters except the stiffness of the elastic element are known. For each combination of the elastic parameters, within the desired range, the trend of $T_i$ is calculated as a function of the bending angle $\theta_i$. A 2-D matrix containing the values of the tension $T_i$ versus the angle $\theta_i$ and the elastic parameters of the $i$th elastic component is obtained. This matrix has to be analyzed and optimized. The following values are obtained:

- the best elastic parameters of the $i$th elastic component (the definition of "best" will be investigated in 4.1.1.)
- the mean values of $T_i$
- the peak values of $T_i$.

The generic output matrix obtained from the study of the $i$th link is a *(N-i+2)-dimensional matrix*.

*4.1.1. Optimization of K.* The calculation of the wire tensions yields a matrix describing the behavior of $T_i$ as a function of the bending angles, defined for the values of the elastic parameters of the $i$th elastic element. The number and typology of the elastic parameters depend on the typology of the elastic components and on its model, e.g., linear torsion springs can be defined using their stiffness and free angle.

Many different possibilities are available for the choice of the best parameters, depending on various constraints and design choices. Some examples are the minimization of the p-norm related to specific Lebesguespaces[28,29] $L_p$:

- Minimization of the $L_\infty$ norm = minimization of the peak value of the signal.
- Minimization of the $L_2$ norm = minimization of the energy of the signal.
- Minimization of the $L_1$ norm = minimization of the total resources of the signal.

Figure 8 represents an example of the result of the optimization of the generic $T_i$. In the specific case the elastic component has been modeled in a similar way to a linear stiffness torsion spring. This spring applies a torque proportional to the angle, but with a fixed target torque for a particular angle (corresponding to point P). The parameters are the stiffness $k_i$ and the free angle $\hat{\theta}_i$. In this example the minimization of the $L_2$ norm of the signal $T_i$ was imposed, i.e., the underlying area of the signal. Figure 8 shows a family of curves; each curve is the trend of $T_i$ for a certain value of $k_i$ and of the corresponding $\hat{\theta}_i$. The horizontal star-dotted line shows the minimum threshold of the tendon tension $T_{min}$ and the thick line corresponds to the curve with the optimized value of $k_i$.

Many other solutions, such as nonlinear springs, discrete elastic elements or other components are equally possible and can be treated in a similar way using their respective transfer functions:
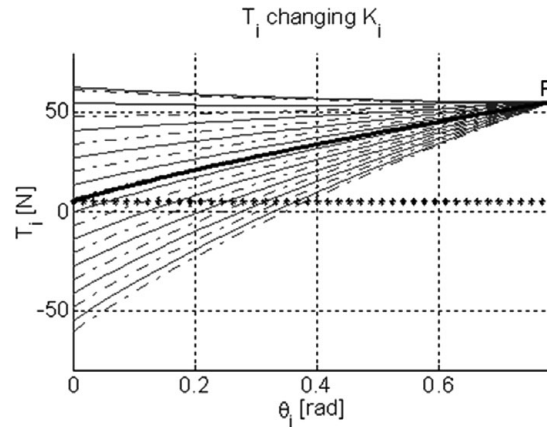
$$C_i = f(\theta_i). \tag{8}$$

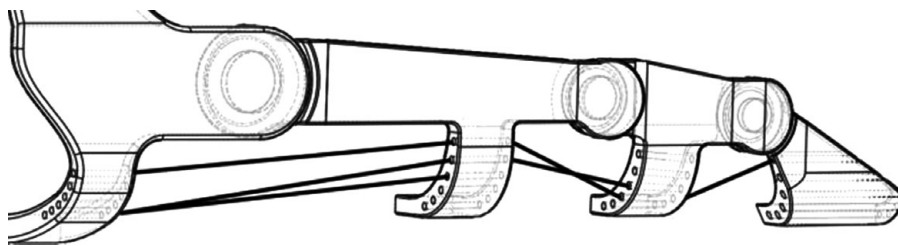Fig. 8. Wire tension with different values of elastic parameters.



Fig. 9. Finger exoskeleton design.

As mentioned above, the elastic elements act in opposition to the tendons. This means that there is an additional design possibility because more rigid elements can be compensated by a larger tendon tension. A good shaping of the transfer function of the elastic elements means that the behavior of the tensions could be modeled by imposing the passage through fixed points, which then modify the peaks and slopes.

*4.1.2. Optimization of the tendon configurations.* Changing the tendon configuration allows us to study the effects of different combinations on internal forces and torques and in particular the tendon tensions. In this way it is possible to find the most suitable combination according to specific design criteria.

At the end of each iteration, the peak and mean values of the three tendon tensions for a specific set of tendon configurations is obtained. The goal is to find the best solution, generally the one that minimizes the demand of the actuators. Depending on the requirements of the specific project, the tendon configuration can aim to minimize different values:

- the peak of tensions:  $\min[\max_i(T_i)]\ i = 1 \dots N$
- the mean of tensions:  $\min[\text{mean}_i(T_i)]\ i = 1 \dots N$

The first results useful to control and limit spikes and overshoots which could damage the tendons or exceed the actuator capability, the second can be useful to reduce as much as possible the power consumption.

## 5. The Specific Case of Exoskeleton Design

### 5.1. The design concepts

Figure 9 depicts a possible design for a finger exoskeleton that follows the general concepts described. The structure is fixed to the palm by a proper support and is composed of three links corresponding to the human phalanges connected by rotary joints. Several holes are present on each phalange to illustrate the possible paths of the wires among which a choice will be made through optimization.
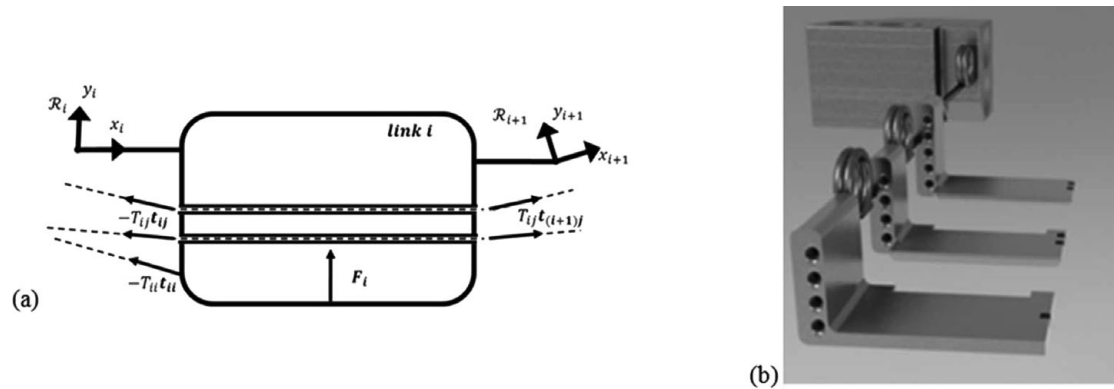
Fig. 10. The specific link design with additional constraints: schematics (a) and CAD model (b).

For model validation, a simplified structure has been conceived in order to allow testing and to compare the theoretical simulation with the experimental results. It fits the following requirements and simplifications;

- all the forces and the vectors defining the geometry lie on the same plane
- three links: $N = 3$
- all wire holes of the $i$th link are parallel to the $i$th x axis
- all wire holes of the $i$th link start and end at the same x coordinate
- no friction: $\varphi_{ij} = 1 \forall i, j$
- the $i$th external force is parallel to the $i$th y axis
- the external forces are tunable parameters because they are targets for control strategies
- negligible weight
- the elastic elements are modeled as linear torsion springs.

Figure 10 shows a schematic representation (a) and a 3-D cad model (b) of the simplified structure defined above. The model shows an asymmetric design composed by three DoF actuated by coplanar tendons, passing through the holes. The joints are torsion springs guaranteeing the extension movement. This solution was chosen in order to minimize the lateral thickness of each phalange; moreover, it does not interfere with the finger crotch in the specific case of the index finger. Different fingers will require different solutions for the MCP articulation. Finally, some constraints on the relative position between two tendons have to be imposed to avoid intersections.

*5.1.1. The finger "soft constraint".* During the study of the characteristics of the human hand, intra- and interfinger constraints were analyzed. These relationships are due to the structure of the hand and the tendon/ligament properties, and couple different DoF. In particular, there is a "soft" constraint between DIP and PIP articulations.[30] This is not a strict kinematic relationship between the two articulations, in fact a partially independent motion on the two phalanges can be forced, but it is valid during normal movements. The relationship is not linear and it is variable among different subjects. However, the constraint is soft and can be partially altered or corrected without causing discomfort; therefore, it has often been approximated with a fixed ratio between the two bending angles:[31,32]

$$\theta_{\text{DIP}} \cong \frac{2}{3} \theta_{\text{PIP}}. \tag{9}$$

The introduction of this constraint inside our algorithm, resulted in a 2-D matrix instead of a 3-D matrix for the tension $T_2$ and to a 3-D matrix instead a 4-D matrix for the tension $T_1$, simplifying calculation and reducing computation time.

*5.2. The elastic elements*
During the static analysis, we introduced the effect of elastic elements with a generic torque $C_i$. The equation and the behavior of $C_i$ depend on the element used to guarantee the extension movement. As mentioned previously, the elastic elements have been modeled as linear torsion springs, with a

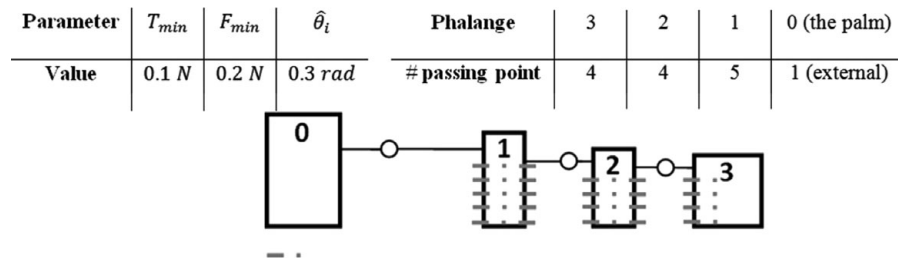| Parameter | $T_{min}$ | $F_{min}$ | $\hat{\theta}_i$ | Phalange | 3 | 2 | 1 | 0 (the palm) |
|-----------|-----------|-----------|------------------|----------|---|---|---|--------------|
| Value | 0.1 N | 0.2 N | 0.3 rad | # passing point | 4 | 4 | 5 | 1 (external) |



Fig. 11. Parameter values and wire holes.

certain free angle and constrained to yield a given torque at a certain bending angle (the fixed point P). The free angle guarantees a certain torque, different from zero, in $\theta_i = 0$ and the fixed point P assures the maximum extension force applied by the EVA glove to the finger.

The equation of the generic elastic element is:

$$C_i = k_i \cdot \left(\theta_i - \theta_i^*\right) + C_i^*, \tag{10}$$

where $\theta_i^*$ and $C_i^*$ come from preliminary studies and tests performed on the EVA glove.[33]

- $\theta_i^*$ is the maximum bending angle of the $i$th articulation wearing the EVA glove;
- $C_i^*$ is the torque applied by the glove to the phalange when it is bent by the angle $\theta_i^*$.

The maximum absolute value of the free angle is guaranteed through the limitation of the minimum value of stiffness $\hat{k}_i$ during the simulation:

$$\hat{k}_i = \frac{C_i^*}{\theta_i^* + \hat{\theta}_i}. \tag{11}$$

### 5.3. Results
Many simulations with different characteristics have been performed. The input parameters defined for each simulation are the following:

- $T_{\min}$: the minimum tendon tensions to always guarantee the control of the movements.
- $F_{\min}$: the minimum contact force between finger and exoskeleton (which becomes the threshold value of the contact force).
- $\hat{\theta}_i$: the free angle of the springs: the material used to build the springs has a finite range of internal stress it can bear. Fixing the value of the free angle (as a function of the material) means that only usable values of the spring parameters can be obtained.
- The acceptable passing points of the holes through the structure and the minimum distance between two adjacent holes, these elements depend on the specific mechanical design of the device.
- The structure of the holes. Reducing the length of the holes, for instance, allows us to simulate the behavior of micropulleys or other design concepts.

In this last paragraph we present two examples of the performed simulations. For these simulations we fixed the parameters values and the discrete passing points of the tendons (shown in Fig. 11) as follows:

In the following part two simulations will be analyzed and, for each one, three different solutions will be presented. In these simulations, the angles $\theta_i$ are considered positive with bending movements, for simplicity, convenience and clarity of interpretation. In each of the following solutions the elastic parameter shave been obtained by minimizing the $L_2$ norm of the tendon tensions, and the best wire configuration has been obtained by minimizing the maximum value of the tendon tensions. For each proposed solution the following outcomes are shown:

- Tendon configurations, describing where the three tendons pass through the different links of the structure.
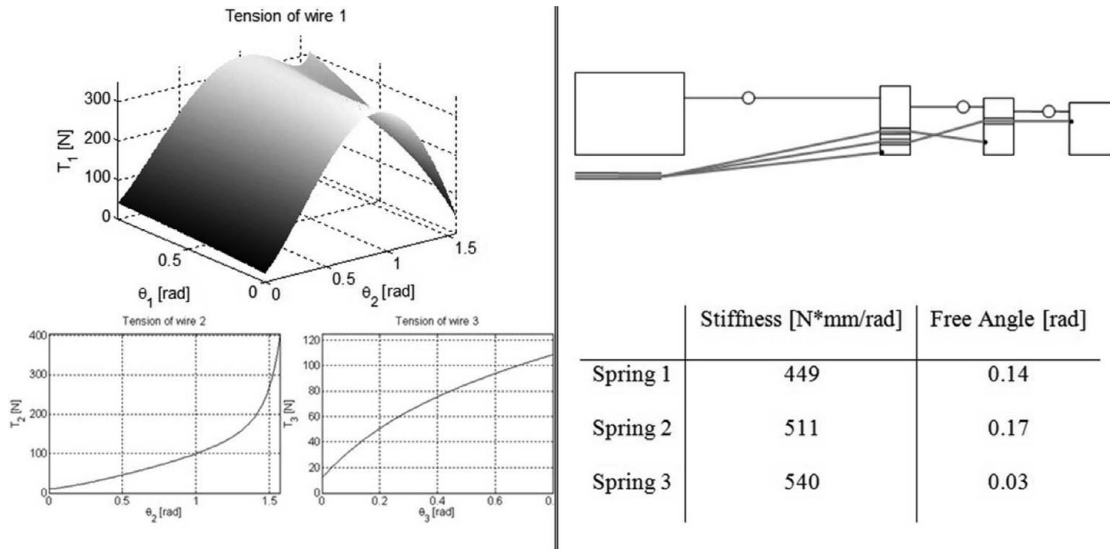
| | Stiffness [N*mm/rad] | Free Angle [rad] |
|---|---|---|
| Spring 1 | 449 | 0.14 |
| Spring 2 | 511 | 0.17 |
| Spring 3 | 540 | 0.03 |

Fig. 12. Solution 1: behavior of the three tendon tensions (left), tendon configuration and elastic parameters (right).



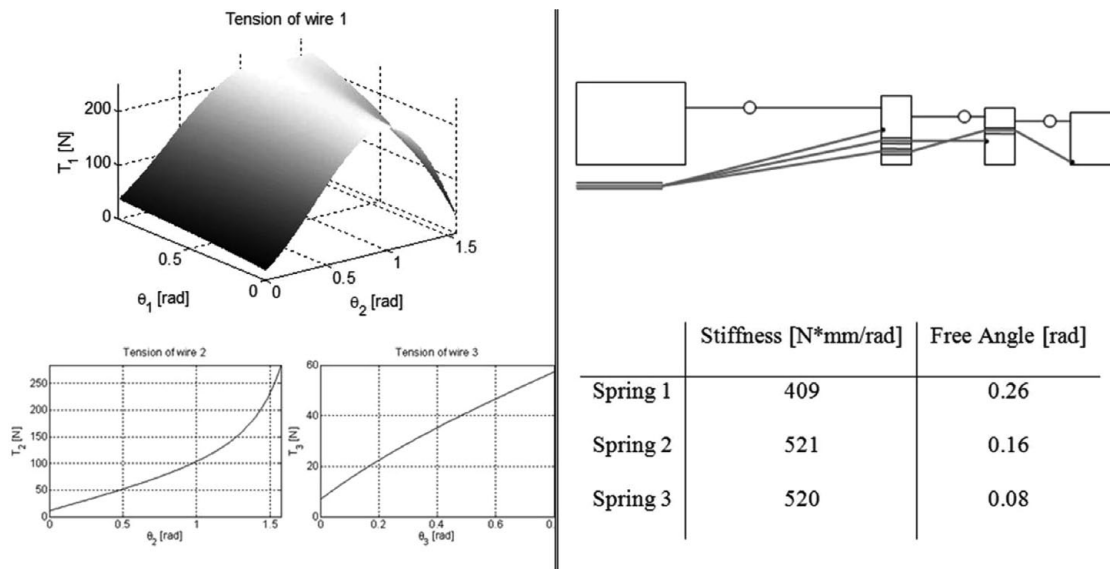| | Stiffness [N*mm/rad] | Free Angle [rad] |
|---|---|---|
| Spring 1 | 409 | 0.26 |
| Spring 2 | 521 | 0.16 |
| Spring 3 | 520 | 0.08 |

Fig. 13. Solution 2: behavior of the three tendon tensions (left), tendon configuration and elastic parameters (right).

- Behavior of the three tendon tensions as a function of the respective bending angles. As stated before the tensions $T_2$ and $T_3$ are functions of only one bending angle so their behavior is shown as a 2-D graph. The tension $T_1$ is a function of two bending angles, thus it is represented through a 3-D graph.
- Maximum and mean values of the three tendon tensions.

*5.3.1. Simulation A: Micromachined holes.* In the first proposed simulation the wires pass through micromachined holes. In this section two nonoptimal solutions (Figs. 12 and 13) are presented as an example, plus the optimal solution (Fig. 14) found with the algorithm.

Table I collects the mean and maximum tension values obtained in the described simulations. It can be noted that the values of the tendon tensions obtained with the optimal solution are sensibly lower. The different values of tension are mainly due to the wire positioning scheme because, as shown in the respective tables, the values of $k$ and $\hat{\theta}$ are very similar.
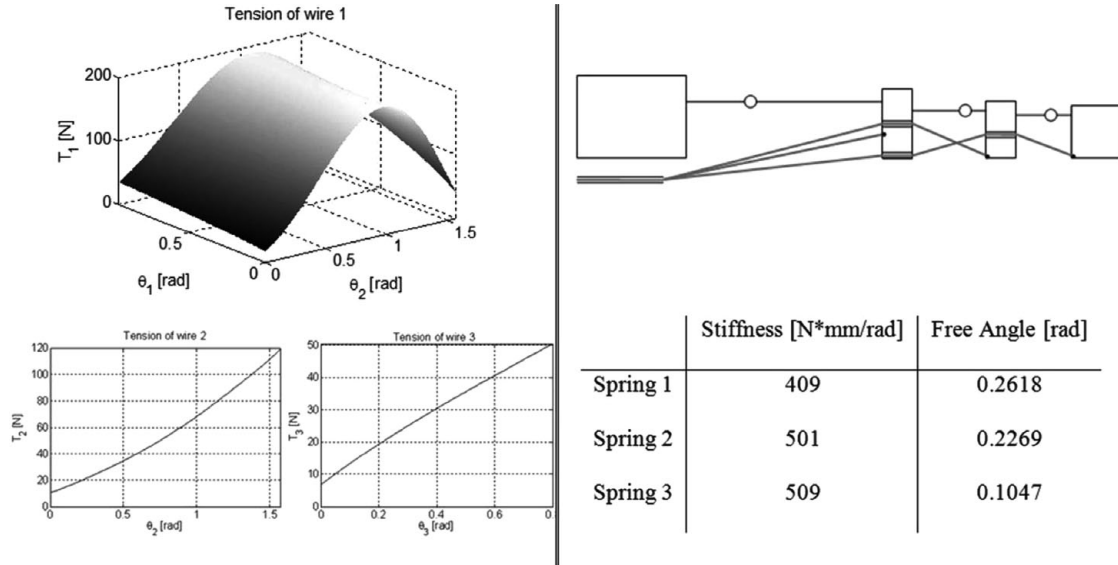
Fig. 14. Optimal solution: behavior of the three tendon tensions (left), tendon configuration and elastic parameters (right).

Table I. Comparison of Maximum and Mean values of the three tendon tensions in the three proposed solutions with micromachined holes.

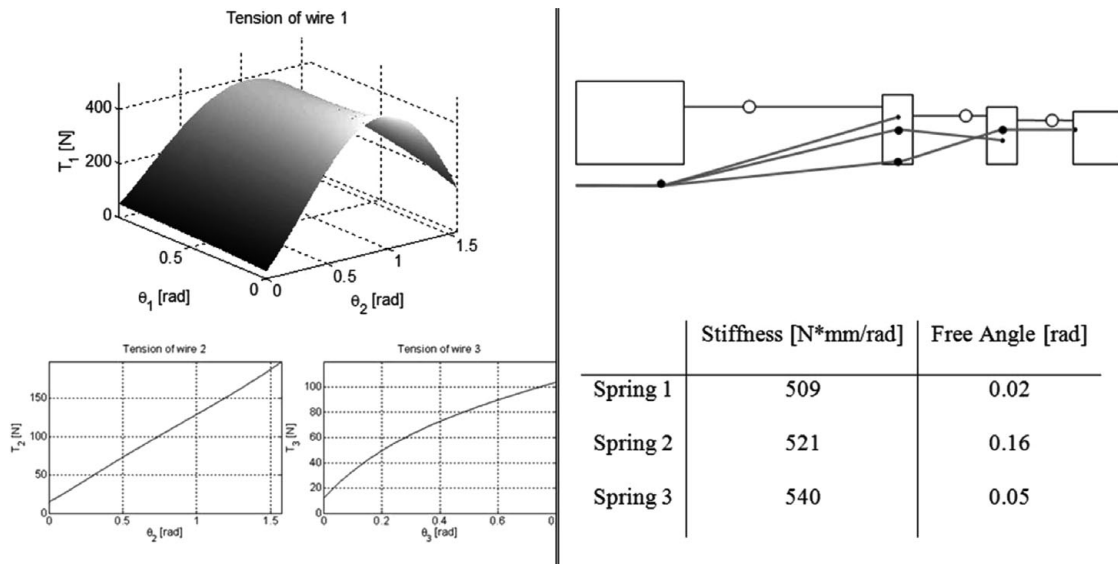|       | Maximum [N] | | | Mean [N] | | |
|-------|-------|-------|------|-------|-------|------|
|       | Sol 1 | Sol 2 | Opt  | Sol 1 | Sol 2 | Opt  |
| $T_1$ | 346   | 222   | 191  | 220   | 145   | 119  |
| $T_2$ | 395   | 277   | 116  | 97    | 92    | 54   |
| $T_3$ | 105   | 56    | 48   | 66    | 32    | 28   |



Fig. 15. Solution 1: behavior of the three tendon tension (left), tendon configuration and elastic parameters (right).
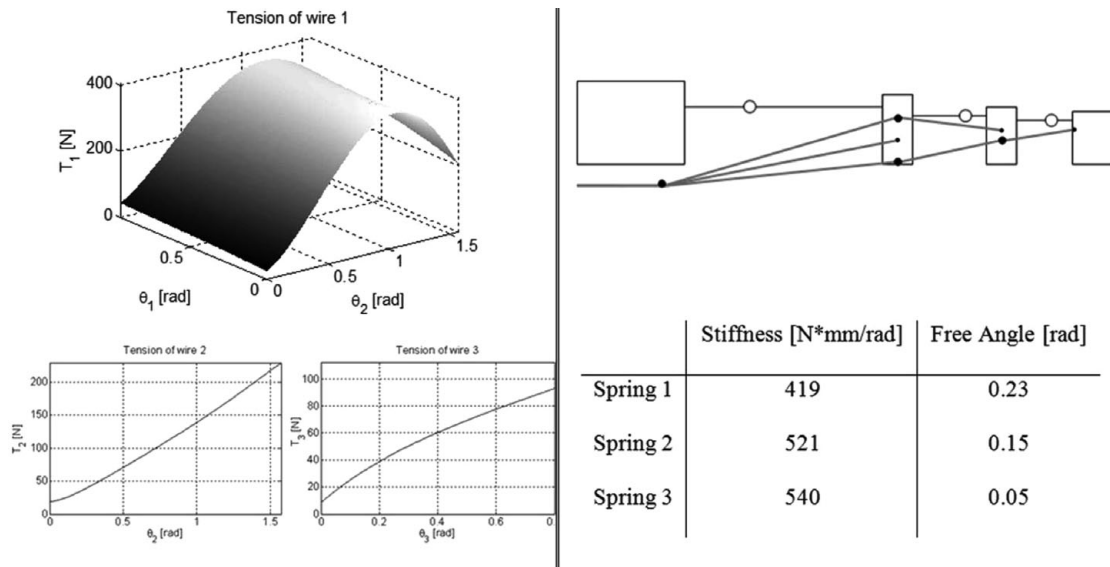
Fig. 16. Solution 2: behavior of the three tendon tension (left), tendon configuration and elastic parameters (right).
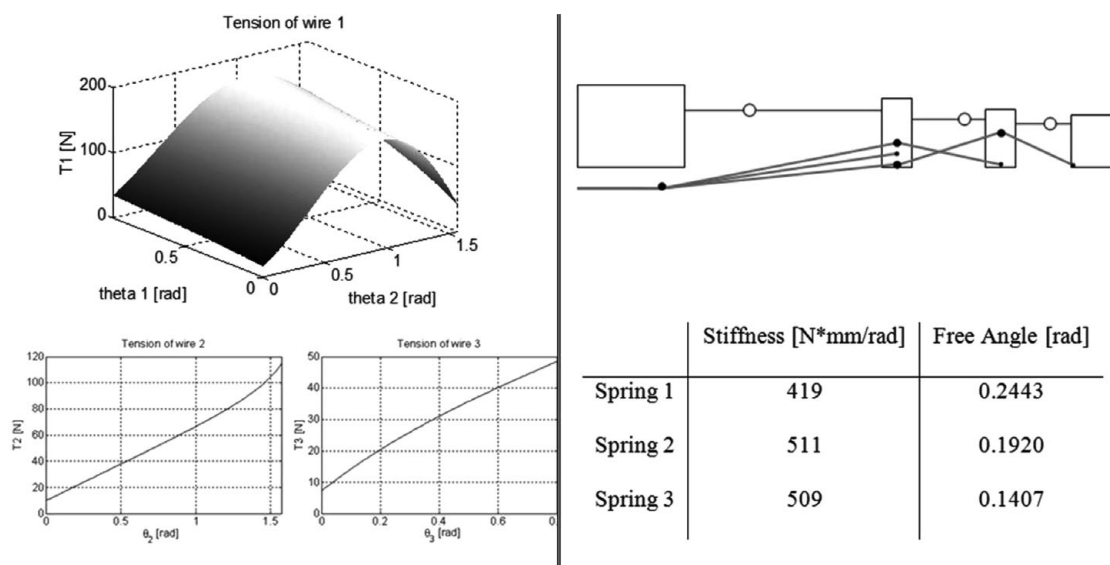


Fig. 17. Optimal solution: behavior of the three tendon tensions (left), tendon configuration and elastic parameters (right).

As mentioned previously each link has an effect on the previous ones. This effect is complex and generally it favors the extension movement of one of the previous phalanges. This can be seen in the increase of the mean value of the tendon tension moving backwards along the kinematic chain.

*5.3.2. Simulation B: Micropulleys.* In the second proposed simulation, the passage of the wires through the structure is done with micropulleys. As in the previous paragraph two nonoptimal solutions (Figs. 15 and 16) and one optimal solution (Fig. 17), calculated with the algorithm, will be presented.

This second simulation confirms the same observations to the first one. With respect to simulation A, the tension values are lower, as can be seen Table II, probably due to the fact that the use of pulleys allows us to obtain longer arms for the forces.

Table II. Comparison of maximum and mean values of the three tendon tensions in the three proposed solutions with micropulleys.

| | Maximum [N] | | | Mean [N] | | |
|---|---|---|---|---|---|---|
| | Sol 1 | Sol 2 | Opt | Sol 1 | Sol 2 | Opt |
| $T_1$ | 475 | 391 | 163 | 280 | 241 | 107 |
| $T_2$ | 193 | 224 | 111 | 100 | 107 | 53 |
| $T_3$ | 100 | 90 | 46 | 63 | 54 | 28 |

## 6. Conclusion

This paper presents the study of a single effect wire actuated n-R robotic structure. The preliminary choices which define the proposed concept stem from dimension and weight constraints related to our specific project, but can be extended to encompass a more general conceptual scheme. The paper provides a procedure which is as general as possible for the analysis and optimization of any single effect structure which has serial kinematics and is actuated by wires, with no direct access to the joint axes. Finally, two simulations with all the geometrical dimensions and characteristics of our specific project are presented. The comparison between the results obtained through the different simulations, show that results can change widely with little variation in the parameters.

## References

1. C. Ferraresi, M. Paoloni and F. Pescarmona, "A new 6-DOF parallel robotic structure actuated by wires: The WiRo-6.3," *J. Robot. Syst.* **21**(11), 581–595 (2004).
2. C. Ferraresi, C. Paoloni and F. Pescarmona, "A new methodology for the determination of the workspace of six-DOF redundant parallel structures actuated by nine wires," *Robotica* **25**(1), 113–120 (2007).
3. K. Maeda, S. Tadokoro, T. Takamori, M. Hiller and R. Verhoeven, "On Design of a Redundant Wire-Driven Parallel Robot WARP Manipulator," *IEEE International Conference on Robotics and Automation*, Detroit, Michigan (1999) pp. 895–900.
4. J. Albus, R. Bostelman and N. Dagalakis, "NIST robocrane," *J. Robot. Syst.* **10**(5), 709–724 (1993).
5. S. Kawamura, W. Choe and S. Tanak, "Development of an Ultrahigh Speed Robot Falcon Using Wire Driven Systems," *IEEE International Conference on Robotic and Automation*, Nagoya, Japan (1995) pp. 215–220.
6. J. P. Merlet, *Parallel Robots*, 2nd ed. (Springer, Netherlands, 2006).
7. J. P. Merlet "Kinematics of the Wire-Driven Parallel Robot Marionet Using Linear Actuators," *International Conference on Robotics and Automation*, Pasadena, California (2008) pp. 3857–3862.
8. M. Gouttefarde, J. P. Merlet and D. Daney, "Wrench.Feasible Workspace of Parallel Cable Driven Mechanism," *International Conference on Robotics and Automation*, Rome, Italy (2007) pp. 1492–1497.
9. "Shadow Dexterous Hand," 18 June 2013 http://www.shadowrobot.com/hand/
10. "Dextrous Robot Hands," 18 June 2013 http://www.dlr.de/rm/en/desktopdefault.aspx/tabid-3802/6102_read-8923/
11. D. Scott and A. Leonov, *Two Sides of the Moon: Our Story of the Cold War Space Race* (Thomas Dunne Books, St. Martin's Griffin, New York, 2006).
12. D. Graziosi, J. Stein, A. Ross and J. Kosmo, "Phase VI Advanced EVA Glove Development and Certification for the International Space Station". SAE Technical Paper 2001-01-2163, 2001, doi:10.4271/2001-01-2163.
13. N. Singh, S. Ariafar and A. Nicolas, "Space Environment Threats and Their Impact in Near Earth Orbits" *Proceedings of the 57th International Astronautical Congress*, Valencia, Spain (Oct. 2–6, 2006).
14. J. M. O'Hara, M. Briganti, J. Cleland and D. Winfield "Extravehicular Activities Limitation Study. Volume II: Establishment of Physiological and Performance Criteria for EVA Gloves" Final Report (Report number ASEVALS- FR-8701), NASA Contract no NAS-9–17702, 1988.
15. R. R. Bishu and G. Klute, "The effects of extra vehicular activity (EVA) gloves on human hand performance," *Int. J. Indust. Ergon.* **16**(3), 165–174 (1995).
16. E. A. Benson, S. A. England, M. Mesloh, S. Thompson and S. Rajulu, "Use of Traditional and Novel Methods to Evaluate the Influence of an EVA Glove on Hand Performance," *ICES 2010*, Barcelona Spain (Jul. 11–15, 2010).
17. A. Favetto, F. Chen, E. P. Ambrosio, D. Manfredi and G. C. Calafiore, "Towards a Hand Exoskeleton for a Smart EVA Glove," *Proceedings of the International Conference on Robotics and Biomimetics*, Tianjin, China (Dec. 14–18, 2010), pp. 1293–1298.
18. C. Dumont, G. Albus, D. K. Meesenburg, J. Fanghänel, K. M. Stürmer and H. Nägerl, "Morphology of the interphalangeal joint surface and its functional relevance," *J. Hand Surg.* **33**(1), 9–18 (2008).

19. A. Chiri, F. Giovacchini, N. Vitiello and E. Cattin, "HANDEXOS: Towards an Exoskeleton Device for the Rehabilitation of the Hand," *Proceedings of the International Conference on Intelligent Robots and Systems*, St. Louis, USA (Oct. 11–15, 2009) pp. 1106–1111.
20. M. DiCicco, L. Lucas and Y. Matsuoka, "Comparison of Control Strategies for an EMG Controlled Orthotic Exoskeleton for the Hand," *Proceedings of the International Conference on Robotics & Automation*, New Orleans, LA (Apr. 26–May 1, 2004) pp. 1622–1627.
21. "Haptics Pictures," 18 June 2013 http://bdml.stanford.edu/twiki/bin/view/Haptics/HapticsPictures.html.
22. G. Berselli, M. Piccinini and G. Vassura, "Comparative Evaluation of the Selective Compliance in Elastic Joints for Robotic Structures," *Proceedings of the IEEE International Conference on Robotics and Automation*, Shanghai, China (May 8–13, 2011) pp. 4626–4631.
23. H. In, D. Lee and K. J. Cho, "Investigation of Friction Characteristics of a Tendon Driven Wearable Robotic Hand," *Proceedings of the International Conference on Control, Automation and Systems*, Gyeonggi-do, Korea (Oct. 27–30, 2010), pp. 568–573.
24. M. Ceccarelli, *Fundamentals of Mechanics of Robotic Manipulation* (Springer, Dordretch, 2004).
25. G. Carbone, E. Ottaviano and M. Ceccarelli, "An optimum design procedure for both serial and parallel manipulators," *IMechE C J. Mech. Eng. Sci.* **221**(7) 829–843, (2007).
26. G. Carbone, E. Ottaviano and M. Ceccarelli, "Optimality Criteria for the Design of Manipulators," *Proceedings of the IEEE Conference on Robotics, Automation and Mechatronics*, Chengdu, China (Sep. 21–24, 2008) pp. 768–773.
27. G. Carbone (Ed.), *GRASPING in Robotics* (Springer, London, 2013).
28. R. G. Bartle, *The Elements of Integration and Lebesgue Measure* (Wiley, New York, 1995).
29. N. Dunford and J. T. Schwartz, *Linear Operators, Part 1: General Theory* (Wiley-Interscience, Hoboken, New Jersey, 1958).
30. J. N. A. L. Leijnse, P. M. Quesada and C. W. Spoor, "Kinematic evaluation of the finger's interphalangeal joints coupling mechanism-variability, flexion-extension differences, triggers, locking swanneck deformities, anthropometric correlations," *J. Biomech.* **43**(12), 2381–2393 (2010).
31. C. S. Fahn and H. Sun, "Development of a data glove with reducing sensors based on magnetic induction," *IEEE Trans. Indust. Electr.* **52**(2), (Apr. 2005) pp. 585–594.
32. S. Cobos, M. Ferre, M. A. Sànchez-Uràn and J. Ortego, "Constraints for Realistic Hand Manipulation," *PPRESENCE 2007, The 10Th Annual International Workshop on Presence*, Barcelona Spain (Oct. 1998).
33. M. Mousavi, S. Appendino, A. Battezzato, F. Chen Chen, A. Favetto and F. Pescarmona, "Stiffness of an EVA Glove: Objective Evaluation and Testing Procedures," *Proceedings of the 12th Symposium on Advanced Space Technologies in Robotics and Automation (ASTRA)* (May 15–17, 2013).